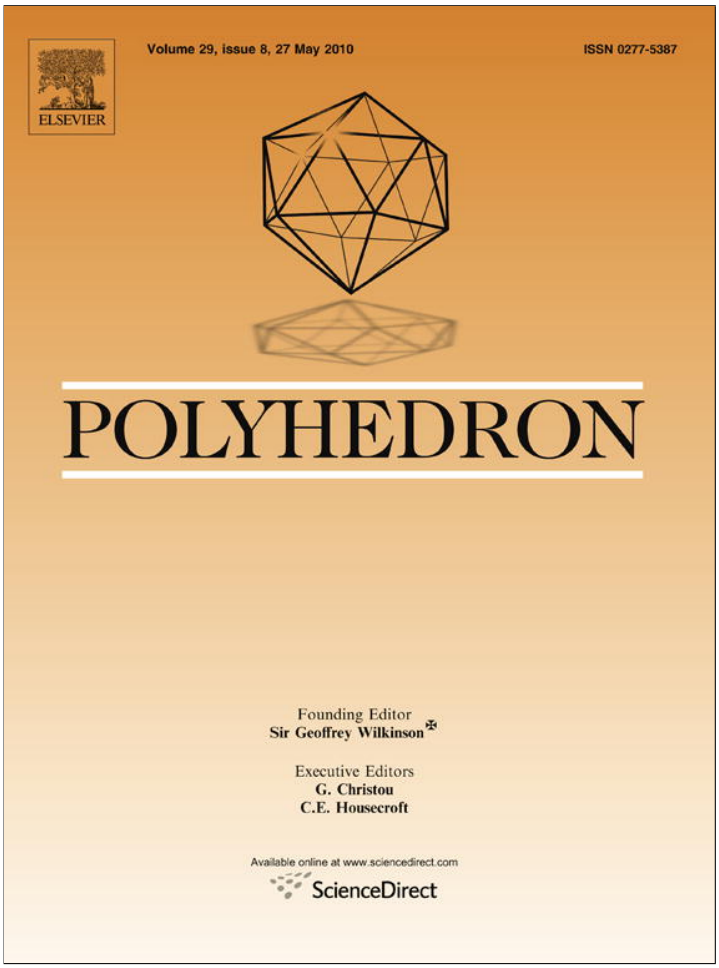

Polyhedron 29 (2010) 1891–1901

Contents lists available at ScienceDirect

Polyhedron

journal homepage: www.elsevier.com/locate/poly

Hemilability of 2-(1H-imidazol-2-yl)pyridine and 2-(oxazol-2-yl)pyridine ligands: Imidazole and oxazole ring Lewis basicity, Ni(II)/Pd(II) complex structures and spectra

Abiodun O. Eseola [a,b,*], Wen Li [c], Olalere G. Adeyemi [a], Nelson O. Obi-Egbedi [b], Joseph A.O. Woods [b,**]

[a] Chemical Sciences Department, Redeemer's University, Redemption City, Km. 46 Lagos–Ibadan Expressway, Nigeria
[b] Inorganic and Physical Chemistry Units, Department of Chemistry, University of Ibadan, Ibadan, Nigeria
[c] Key Laboratory of Photochemical Conversion and Optoelectronic Materials, Technical Institute of Physics and Chemistry, The Chinese Academy of Sciences, Beijing 100190, China

ARTICLE INFO

Article history:
Received 19 January 2010
Accepted 26 February 2010
Available online 12 March 2010

Keywords:
Hemilability
Lewis basicity
Protonation–deprotonation
Self-assembly
Substituent effects
DFT calculations

ABSTRACT

Fourteen new organic molecules **A1**–**A4**, **B1**–**B5**, **C1**–**C4** and **D** and a series of transition metal(II) complexes (**Ni1**–**Ni9** and **Pd1**–**Pd2b**) were synthesized and studied in order to characterize the hemilability of 2-(1H-imidazol-2-yl)pyridine and 2-(oxazol-2-yl)pyridine ligands (**A1**–**A4** = 2-R^2-6-(4,5-diphenyl-1R^1-imidazol-2-yl)pyridines, R^1 = H or CH_3, R^2 = H or CH_3; **B1**–**B5** = 1-R^2-2-(pyridin-2-yl)-1R^1-phenanthro[9,10-d]imidazoles/oxazoles, R^1 = H or CH_3, R^2 = H or CH_3; **C1**–**C4** = 2-(6-R^2-pyridin-2-yl)-1H-imidazo/oxazo[4,5-f][1,10]phenanthrolines, R^2 = H or CH_3; **D** = 2-mesityl-1H-imidazo[4,5-f][1,10]phenanthroline). They were also used to study the substituent effects on the donor strengths as well as the coordination chemistries of the imidazole/oxazole fragments of the hemilabile ligands.

All the observed protonation–deprotonation processes found within pH 1–14 media pertain to the imidazole or oxazole rings rather than the pyridyl Lewis bases. The donor characteristics of the imidazole/oxazole ring can be estimated by spectroscopic methods regardless of the presence of other strong N donor fragments. The oxazoles possessed notably lower donor strengths than the imidazoles. The electron-withdrawing influence and capacity to hinder the azole base donor strength of 4,5-azole substituents were found to be in the order phenanthrenyl (**B** series) > 4,5-diphenyl (**A** series) > phenanthrolinyl (**C** series). An X-ray structure of **Ni5b** gave evidence for solvent induced ligand reconstitution while the structure of **Pd2b** provided evidence for solvent induced metal–ligand bond disconnection.

Interestingly, alkylation of 1H-imidazoles did not necessarily produce the anticipated push of electron density to the donor nitrogen. Furthermore, substituents on the 4,5-carbons of the azole ring were more important for tuning donor strength of the azole base. DFT calculations were employed to investigate the observed trends. It is believed that the information provided on substituent effects and trends in this family of ligands will be useful in the rational design and synthesis of desired azole-containing chelate ligands, tuning of donor properties and application of this family of ligands in inorganic architectural designs, template-directed coordination polymer preparations, mixed-ligand inorganic self-assemblies, etc.

1. Introduction

Research efforts on the science and application of intermolecular or intramolecular hydrogen bonding interactions are still receiving attention [1–3]. Investigations on hydrogen-bonded species of relatively simple molecules is routinely applied towards understanding protonation–deprotonation and proton/electron transfer mechanisms of complicated systems [4,5]. Imidazole and oxazole compounds have drawn considerable attention for their desirable properties in the fields of coordination chemistry, photoluminescence/pH sensing studies, biochemistry of metalloenzymes, medicinal chemistry, etc. [6–12]. Moieties such as adenine, guanine, and histidine, contain the imidazole ring and are involved in intramolecular and/or intermolecular chemistries of biological macromolecules under pH specific conditions [1,13–15]. The imidazole fragment of histidine is recognized to be an interesting ligand in the bioinorganic chemistry of most hemoproteins and studies on the basicity and steric effects using synthetic imidazole compounds provide an understanding of the roles played by such donor fragments in biochemical reaction mechanisms [10,14,15].

* Corresponding author at: P.M.B. 3005, Redemption City, Ogun, Nigeria. Tel.: +230 (0) 7062192104.
** Corresponding author. Tel.: +234 (0) 8060156565.
E-mail addresses: bioduneseola@run.edu.ng (A.O. Eseola), jao.woods@mail.ui.edu.ng, jaowoods@yahoo.com (J.A.O. Woods).

0277-5387/$ - see front matter © 2010 Elsevier Ltd. All rights reserved.
doi:10.1016/j.poly.2010.02.039

Ligand chemical recognition is an important phenomenon in the science of inorganic coordination polymers and supramolecular self-assembly complex architectures, which are rapidly expanding structural chemistry fields, and it is possible to control 3-D structures by rational ligand framework modifications as well as by careful selection of the metal ion [16–21]. Ligand exchange processes, which are dependent on relative ligand field strengths and/or steric requirements of leaving and incoming ligands, are very important in the synthetic chemistry of coordination complexes [22–24]. Therefore, knowledge of lability is important towards the successful execution of template-directed coordination polymer preparations or ligand exchange reactions [25–30]. The general conclusions from isolated cases report that the N donors of azoles possess pK_a values ≈ 6–9, which are within the pH scale [31–34]. However, on account of substituent effects, a variation of pK_a in the range 1.1–6.4 was obtained in our recent studies on a series of new 2-(1H-imidazol-2-yl)phenols in which distant phenol ring substituents were observed to be more effective in tuning the basicity of the imidazole fragment [35]. Among the azole ligands, imidazoles are more attractive due to the anticipated opportunities of directly modifying the electronic nature of the imidazole N donor through substitution of the active imidazole proton [36]. For instance, an attempt to modifying electrophilicity of transition metal active sites towards olefin homogeneous polymerization through imidazole proton alkylation was recently reported [37]. Furthermore, imidazole ligands could also find application in surface chemistry because they can be immobilized on solid supports through the imidazole proton [38].

Works concerning azole donor chelate ligands have been largely restricted to benzo[*d*]imidazoles, benzo[*d*]oxazoles and benzo[*d*]thiazoles [11,33,34,37]. Despite the considerable interest in azole ligands, a systematic investigation of substituent effects on the azole ring donor characteristics is still lacking. The concept of combining hard and soft donors such as N–P, into the same chelator is of current interest [39], but azole based chelators are yet to be characterized or exploited as hemilabile ligands. Primarily, the interest in this work resulted from observed lability of metal complexes of some bidentate 2-(1H-imidazol/oxazol-2-yl)phenols and 2-(1H-imidazol/oxazol-2-yl)pyridines during attempts to prepare their Zn(II) and Ni(II) complexes, respectively, despite expected chelate effects [40,41]. For some of the ligands, coordination was difficult to attain or solvent molecules, such as methanol, readily and completely detached the weakly chelating imidazole/oxazole ligands.

Spectroscopic determination of ionization constants of weak acids or bases is of widespread application and considered suitable even under extremes of pH, poor solute solubilities and for species prone to conformational photo-tautomerism [42,43]. For instance, the pK_a of a drug is one of the most important parameters employed to explain its physicochemical activities, acid–base properties and design of pharmaceutical pre-formulations [44]. Ionization constants of organic materials are strongly solvent dependent [45,46]. Our aim in this work was to study the trends in inherent electronic properties by subjecting a series of related organic bases to the same media conditions. Aqueous-organic mixtures are often employed at various pH for ionization constant determinations [44]. Computational works, largely restricted to 2-(1H-benzo[d]imidazol-2-yl)phenols, are known and the B3LYP/6-311+G* basis set has been successfully employed as a reliable method in DFT calculations of imidazole-containing organic systems [47–49].

Herein, we present our results on the syntheses and comparative studies of substituent effects on imidazole/oxazole Lewis base donor characteristics for a series of new, hemilabile 2-(1H-imidazol-2-yl)pyridines/2-(oxazol-2-yl)pyridines (Scheme 1). For comparison, 2-mesityl-1H-imidazo[4,5-f][1,10]phenanthroline (**D**) was also prepared and studied. Spectroscopic properties of the dihalo Ni(II) complexes (**Ni1**–**Ni9**) and dichloro Pd(II) complexes (**Pd1** and **Pd2a**), resulting from coordination of the respective M(II) halides with members of the **A** and **B** ligand series, were examined for clues on ligand donor characteristics. He X-ray structures of **Ni5b** and **Pd2b** are also presented as further evidence for the observed trends. The calculated properties, based on optimized geometries of the ligand molecules, and experimental ^{1}H NMR and FTIR data of the imidazole active protons were obtained and discussed in an attempt to rationalize the experimentally observed ligand properties.

2. Experimental

2.1. General considerations

All manipulations of oxidation-prone reactions were performed under a nitrogen atmosphere using standard Schlenk techniques. All starting materials were obtained commercially as reagent grade and were used without further purification. Compounds **A1**–**A4**, **B1**, **B2**, **B4** and **Ni1**–**Ni9** were prepared according to recently published procedures [41]. 1,10-Phenanthroline-5,6-dione was synthesized according to a known method [50]. The synthesized organic compounds were purified on a silica gel column to exclude impurities. Elemental analyses were performed on a Flash EA 1112 microanalyzer, CE Instruments. ^{1}H and ^{13}C NMR spectra were recorded on a Bruker ARX-400 MHz instrument using deuterated chloroform as the solvent and TMS as an internal standard. IR spectra were recorded on a Nicolet 6700 FTIR spectrometer or Shimadzu 8740 FTIR spectrometer as KBr discs in the range 4000–400 cm^{-1}. UV–Vis measurements were recorded on Shimadzu 1600 spectrophotometer. The pK_a determination experiments were carried out using ≈ 10^{-5} M solutions of the compounds in an ethanol–water mixture which consisted of 70% absolute EtOH and 30% H_2O. A calculated amount of potassium chloride was used to achieve the 0.1 M concentration of the salt in order to maintain a fairly constant ionic strength. The adjustment of the pH of solutions was achieved through the addition of potassium hydroxide or hydrochloric acid solutions and monitored with the aid of a calibrated pH meter. The pH measurements were made on an Omega

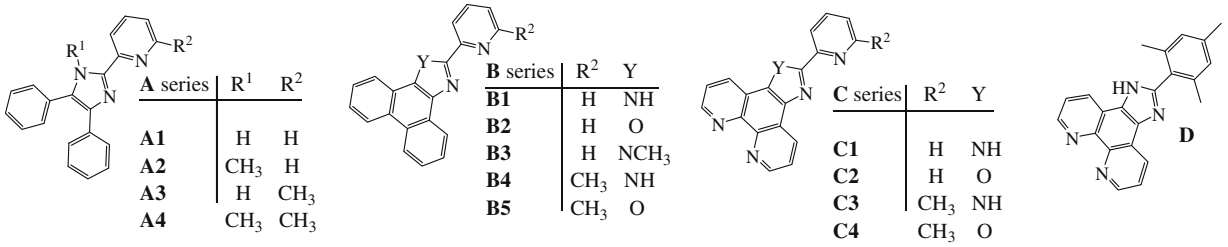

Scheme 1. Ligand frameworks investigated in this work.

PHB-212 Microprocessor pH Meter using buffers of pH 4.0 and 9.2 as calibrants. Optimized geometries and calculated properties were obtained by DFT calculations conducted at the B3LYP/6-311+G* level using the GAUSSIAN 98 package of programs [51]. Input files were created based on simulated dielectric constants for a 70% ethanol–water mixture.

2.2. Preparation of imidazoles/oxazoles

2.2.1. 1-Methyl-2-(pyridin-2-yl)-1H-phenanthro[9,10-d]imidazole (**B3**)

2-(Pyridin-2-yl)-1H-phenanthro[9,10-d]imidazole (0.50 g, 1.693 mmol) and K_2CO_3 (0.47 g, 3.39 mmol) were refluxed in acetonitrile for 10 min followed by addition of iodomethane (0.2 mL, ≈1.5 equiv.). Refluxing was continued for 10 h. The reaction flask was cooled and the solvent removed under vacuum. The residue was extracted with 100 mL dichloromethane and the organic solvent was removed under vacuum. The crude product was purified over silica gel with 15:5:1 petroleum ether/ethyl acetate/acetone as eluent to obtain the white micro-crystalline compound **B3** (0.21 g, 40%). M.p. 204–206 °C. Selected IR peaks (KBr disc, cm^{-1}): ν 3041m, 2947m, 1607m, 1583s, 1454vs, 1237m, 799s, 752vs. ^1H NMR (δ, ppm): 8.84 (d, J = 7.97 Hz, 1H); 8.79 (d, J = 7.88 Hz, 1H); 8.74 (d, J = 4.71 Hz, 1H); 8.70 (d, J = 8.26 Hz, 1H); 8.57 (d, J = 8.11 Hz, 1H); 8.44 (d, J = 7.924 Hz, 1H); 7.91 (dd, J = 7.77 Hz, 1H); 7.66 (m, 4H); 7.37 (dd, J = 4.9 Hz, 1H); 4.75 (s, 3H). *Anal.* Calc. for $C_{21}H_{15}N_3$: C, 81.53; H, 4.89; N, 13.58. Found: C, 81.29; H, 4.92; N, 13.50%.

2.2.2. 2-(6-Methylpyridin-2-yl)phenanthro[9,10-d]oxazole (**B5**)

Phenanthrenequinone (1.00 g, 4.803 mmol) and 6-methylpyridine-2-carboxaldehyde (0.64 g, 5.283 mmol) were refluxed in a chloroform (5 mL)/ethanol (5 mL) mixture for 3 h in the presence of ammonium acetate (7.40 g, 96.006 mmol) and glacial acetic acid (0.5 mL) as a catalyst. The reaction solution was cooled and stirred with a few drops of concentrated aqueous ammonia at room temperature to neutralize residual acid. The mixture was extracted twice with dichloromethane (60 mL and 20 mL) and the combined organic extract was concentrated under vacuum. The crude mixture was purified by column chromatography on a silica gel column using petroleum ether/dichloromethane (1:4) as the eluent. The eluent portion containing the product was collected and concentrated under vacuum. Addition of petroleum ether precipitated **B3** as microcrystalline needles which were filtered washed with petroleum ether and dried under vacuum at 60 °C (0.43 g, 28.3%). M.p. 199–201 °C. Selected IR peaks (KBr disc, cm^{-1}): ν 3061s, 1616s, 1591s, 1569vs, 1459vs, 1429vs, 1233vs, 1080vs, 798vs, 761vs. ^1H NMR (400 MHz, TMS, $CDCl_3$) (δ, ppm): 8.75 (m, 3H, phenanthrene); 8.47 (d, J = 8.03 Hz, 1H, phenanthrene); 8.28 (d, J = 7.78 Hz, 1H, py); 7.83 (dd, J = 7.77 Hz, 1H, py); 7.73 (m, 4H, phenanthrene); 7.33 (d, J = 7.72 Hz, 1H, py); 2.79 (s, 3H, Me). ^{13}C NMR (100 MHz, $CDCl_3$) (δ, ppm): 160.96, 159.58, 150.02, 145.72, 145.57, 137.22, 135.59, 129.77, 129.11, 127.48, 127.27, 126,82, 126.36, 126.18, 124.97, 123.71, 123.40, 123.29, 121.47, 121.03, 120.33, 24.77. *Anal.* Calc. for $C_{21}H_{14}N_2O\cdot(^4/_5)H_2O$: C, 77.66; H, 4.84; N, 8.63. Found: C, 77.48; H, 4.85; N, 8.65%.

2.2.3. 2-(Pyridin-2-yl)-1H-imidazo[4,5-f][1,10]phenanthroline (**C1**) and 2-(pyridin-2-yl)oxazolo[5,4-f][1,10]phenanthroline (**C2**)

1,10-Phenanthroline-5,6-dione (5.00 g, 0.024 mol), ammonium acetate (37 g, 0.480 mol), glacial acetic acid as a catalyst (1 mL) and 2-pyridinecarboxaldehyde (2.86 mL, 0.030 mol) were reacted according to the procedure for **B5** above, except that the crude mixture was purified on a silica gel column using ethanol/ethylacetate/petroleum ether (1:10:10) as the eluent. The portions that contained the pure products were concentrated and the precipitates were filtered, washed with small amount of ethanol and dried to afford isolated products of **C1** (2.60 g, 36.4%) and **C2** (0.67 g, 9.4%) as white powders. Characterization data are as follows:

C1: M.p. >300 °C. Selected IR peaks (KBr disc, cm^{-1}): ν 3008 m, 2944 m, 1590s, 1562s, 1431vs, 1070 m, 738vs. ^1H NMR (400 MHz, TMS, $CDCl_3$) (δ, ppm): 11.60 (br, s, 1H); 9.17 (d, J = 4.0 Hz, 2H); 9.05 (d, J = 8.0 Hz, 1H); 8.67 (d, J = 4.4 Hz, 1H); 8.52 (d, 7.6 Hz, 1H); 8.45 (d, J = 8.0 Hz, 1H); 7.92 (dd, J = 8 Hz, 1H); 7.74 (dd, J = 4.4, 8.0 Hz, 1H); 7.68 (dd, J = 4.4, 8.0 Hz, 1H); 7.39 (dd, J = 7.6 Hz, 1H). ^{13}C NMR (100 MHz, $CDCl_3$) (δ, ppm): 149.82, 149.17 148.84, 148.78, 148.05, 144.95, 144.78, 137.48, 137.35, 130.34, 128.85, 125.79, 124.40, 123.40, 122.84, 121.26, 118.95. *Anal.* Calc. for $C_{18}H_{11}N_5\cdot\frac{1}{2}H_2O$: C, 70.58; H, 3.95; N, 22.86. Found: C, 70.96; H, 3.66; N, 22.93%.

C2: M.p. 269–271 °C. Selected IR peaks (KBr disc, cm^{-1}): ν 3053s, 2982m, 1584m, 1560m, 1456vs, 1446vs, 1059s, 741vs. ^1H NMR (400 MHz, TMS, $CDCl_3$) (δ, ppm): 9.26 (d, J = 3.8 Hz, 2H); 9.03 (dd, J = 1.7, 8.1 Hz, 1H); 8.91 (d, J = 4.5 Hz, 1H); 8.82 (dd, J = 1.7, 8.1 Hz, 1H); 8.47 (d, J = 7.9 Hz, 1H); 7.97 (dd, J = 7.9 Hz, 1H); 7.97 (m, 2H); 7.51 (dd, J = 4.8, 7.5 Hz, 1H). ^{13}C NMR (100 MHz, $CDCl_3$) (δ, ppm): 162.09, 150.47, 150.02, 149.82, 145.73, 145.19, 145.07, 144.04, 137.22, 134.77, 130.86, 129.01, 125.53, 123.64, 123.38, 123.25, 122.94, 117.97. *Anal.* Calc. for $C_{18}H_{10}N_4O\cdot\frac{1}{2}H_2O$: C, 70.35; H, 3.61; N, 18.23. Found: C, 70.52; H, 3.65; 18.20%.

2.2.4. 2-(6-Methylpyridin-2-yl)-1H-imidazo[4,5-f][1,10]phenanthroline (**C3**) and 2-(6-methylpyridin-2-yl)oxazolo[5,4-f][1,10]phenanthroline (**C4**)

1,10-Phenanthroline-5,6-dione (3.00 g, 0.014 mol), ammonium acetate (22 g, 0.29 mol) and 6-methylpyridine-2-carboxaldehyde (2.1818 g, 1.25 equiv.) were reacted according to the procedure for **C1** and **C2** above to obtain **C3** (1.10 g, 24.5%) and **C4** (0.37 g, 8.2%) as light yellow and purple micro-crystals, respectively.

C3: Mp. >300 °C. Selected IR peaks (KBr disc, cm^{-1}): ν 3057s, 3016s, 1590m, 1562s, 1440s, 1068s, 739vs. ^1H NMR (400 MHz, TMS, $CDCl_3$ (δ, ppm): 11.60 (br, s, 1H); 9.17 (d, J = 4.1 Hz, 2H); 9.05 (d, J = 8.2 Hz, 1H); 8.49 (d, J = 7.7 Hz, 1H); 8.52 (d, 7.6 Hz, 1H); 8.30 (d, J = 8.0 Hz, 1H); 7.80 (dd, J = 7.7 Hz, 1H); 7.74 (dd, J = 4.4, 8.0 Hz, 1H); 7.68 (dd, J = 4.4, 8.0 Hz, 1H); 7.24 (d, partially overlapped with a $CDCl_3$ residual peak, 1H); 2.66(s, 3H). *Anal.* Calc. for $C_{19}H_{13}N_5$: C, 72.25; H, 4.31; N, 22.17. Found: C, 72.47; H, 4.26; N, 22.05%.

C4: M.p. 266–268 °C. Selected IR peaks (KBr disc, cm^{-1}): ν 3016s, 1587s, 1558s, 1459vs, 1062s, 739vs. ^1H NMR (400 MHz, TMS, $CDCl_3$ (δ, ppm): 9.27 (dd, J = 2.0, 5.7 Hz, 2H); 9.05 (dd, J = 2.1, 10.8 Hz, 1H); 8.02 (dd, J = 2.1, 10.9 Hz, 1H); 8.28 (d, J = 10.3 Hz, 1H); 7.80 (m, 3H); 7.38 (d, J = 10.3 Hz, 1H); 2.79 (s, 3H). ^{13}C NMR (100 MHz, $CDCl_3$) (δ, ppm): 162.50, 159.85, 150.03, 149.75, 145.24, 145.09, 144.07, 137.40, 134.87, 131.20, 129.21, 125.54, 123.65, 123.40, 123.07, 120.62, 118.09, 24.79. *Anal.* Calc. for $C_{19}H_{12}N_4O$: C, 73.07; H, 3.87; N, 17.94. Found: C, 72.98; H, 3.85; N, 17.87%.

2.2.5. 2-Mesityl-1H-imidazo[4,5-f][1,10]phenanthroline (**D**)

1,10-Phenanthroline-5,6-dione (0.50 g, 2.37 mmol), mesitaldehyde (0.35 g, 2.37 mmol), ammonium acetate (3.65 g, 47.40 mmol) and glacial acetic acid (10 mL) were heated under reflux conditions for 2 h, followed by cooling, dilution in ≈20 mL water and neutralization with concentrated aqueous ammonia solution. The crude product was filtered off as a yellow precipitate which was recrystallized from ethanol to obtain compound **D** as microcrystals (0.75 g, 93%). M.p./Dec. >300 °C. Selected IR peaks (KBr disc, cm^{-1}): ν 3272vs, 3061s, 1610m, 1542s, 1454s, 741s. ^1H NMR (400 MHz, TMS, $CDCl_3$) (δ, ppm): 8.85 (d, 4H); 7.46 (br, s, 2H); 6.65 (s, 2H); 2.19 (s, 3H); 1.93 (s, 6H). ^{13}C NMR (TMS, $CDCl_3$) (δ,

ppm): 151.24, 147.69, 143.87, 139.12, 137.83, 130.54, 127.97, 127.56, 123.03, 21.15, 19.90. *Anal.* Calc. for $C_{22}H_{18}N_4{\cdot}2H_2O$: C, 70.57; H, 5.92; N, 14.96. Found: C, 70.74; H, 5.74; N, 14.59%.

2.3. Preparation of Pd(II) complexes

2.3.1. Dichloro{2-(pyridin-2-yl)-1H-phenanthro[9,10-d]imidazole} palladium(II) (*Pd1*)

Using freshly distilled dichloromethane as the solvent, a solution of **B1** (0.15 g, 0.51 mmol) in 20 mL solvent was added dropwise into a solution of $PdCl_2{\cdot}2CNCH_3$ (0.13 g, 0.51 mmol) in 10 mL of solvent, and the resulting reaction mixture was stirred at room temperature for 12 h. The crude product of **Pd1** was filtered as an orange powder, washed with diethyl ether and dried under vacuum at 60 °C. Selected IR peaks (KBr, cm^{-1}): ν 3489, 3396, 3076, 2968, 1611, 1529, 1473, 1458, 1448, 1159, 774, 758, 721. *Anal.* Calc. for $C_{20}H_{15}Cl_2N_3OPd$ (as the monohydrate): C, 48.96; H, 3.08; N, 8.56. Found: C, 48.77; H, 3.22; N, 8.22%.

2.3.2. Dichloro[2-(pyridin-2-yl)phenanthro[9,10-d]oxazole] palladium(II) (*Pd2a*, *Pd2b*)

B2 (0.11 g, 0.39 mmol.) and $PdCl_2{\cdot}2CNCH_3$ (0.10 g, 0.39 mmol) were reacted in the same manner as for the preparation of **Pd1** above to obtain **Pd2a** as yellow micro-needles in 83.1% yield. **Pd2b** was obtained as blocks of brown crystals by standing **Pd2a** in dimethylsulfoxide (DMSO) for a few days. Selected IR peaks (KBr, cm^{-1}): ν 3079, 3052, 1638, 1617, 1546, 1515, 1478, 1434, 1389, 1264, 1097, 771, 721. *Anal.* Calc. for $C_{20}H_{12}Cl_2N_2OPd{\cdot}½H_2O$: C, 49.77; H, 2.71; N, 5.80. Found: C, 49.77; H, 2.63; N, 6.11%.

2.4. X-ray experiments

Suitable crystals of **Ni5b** were obtained by slow diffusion of diethyl ether into a methanol solution of **Ni5a**. Single crystals of **Pd2b** were grown by dissolution of **Pd2a** in DMSO followed by layering with MeOH. X-ray diffraction measurements for complexes **Ni5b** and **Pd2b** were done on a Rigaku R-AXIS Rapid IP diffractometer with graphite monochromated Mo Kα radiation (λ = 0.71073 Å). Intensities were corrected for Lorentz and polarization effects and empirical absorption. The direct method was applied in solving the structural data and refinement was done by full-matrix least squares on F^2. All non-hydrogen atoms were refined anisotropically. All hydrogen atoms were placed in calculated positions. Structure solution and refinement were performed using the SHELXL-97 package [52].

3. Results and discussion

3.1. Absorption properties and protonation states

Table 1 contains the spectral and pK_a data for the investigated ligands. The different protonation states observed within pH 0–14 (three for 1H-imidazole ligands and two for the other ligands) afforded species with different absorption band positions and/or shapes (Fig. 1). Compounds that lacked the 1H-imidazole active proton (*N*-methyl substituted ligands: **A2**, **A4**, **B3**; oxazoles: **B2**, **B5**, **C2** and **C4**; Table 1) gave no change in absorption properties in the pH 6–14 range. Generally, absorption bands were red-shifted in going from acidic through neutral to basic media. Use of spectroscopic methods in quantifying the concentrations of

Table 1
Experimental FTIR, ^{1}H NMR, UV absorption and pK_a data of the studied imidazole molecules.

Compounds	FTIR and NMR signals		λ_{max} (nm) [ε (dm^3/mol cm)][a]			Ionization constant	
	ν_{N-H} (cm^{-1})[b]	^{1}H δ_{N-H} (ppm)[c]	Cation	Neutral	Anion	p$K_{a,N:}$ ± S[e]	p$K_{a,NH}$ ± S[e]
A1	3422m (br)	10.56 [br]	311 [22 500]	323 [24 180]	336 ε[d]	3.71 ± 0.05	>13.90
A2	NA	NA	284 [28 510]	305 [27 490]		3.33 ± 0.02	
A3	3429m (br)	10.39 (br)	314 [23 960]	326 [24 120]	334 ε[d]	3.75 ± 0.07	>14.00
A4	NA	NA	296 [25 570]	306 [25 520]		3.63 ± 0.15	
B1	3433vs (sh)	11.15 (sh)	353 [27 560]	362 [34 360]	382 [25 120]	2.89 ± 0.02	13.26 ± 0.02
B2	NA	NA	390 ε[d]	359 [18 080]		<0.83 ± 0.16	
B3	NA[e]	NA[e]	345 [12 570]	356 [10 260]		2.71 ± 0.10	
B4	3436vs (sh)	11.17 (br)	350 [18 520]	363 [23 420]	382 [15 410]	2.97 ± 0.07	14.08 ± 0.61
B5	NA	NA	390 ε[d]	359 [22 980]		<1.26 ± 0.08	
C1	3120m [br]	11.48 [br]	303 [54 810]	323 [33 780]	338 [35 910]	4.36 ± 0.10	10.06 ± 0.13
C2	NA	NA	290 [52160]	323 [33 500]		2.92 ± 0.05	
C3	3120m [br]	11.39 [br]	304 [41670]	324 [27 450]	337 [29 220]	4.31 ± 0.17	10.73 ± 0.16
C4	NA	NA	289 [50980]	325 [34 210]		2.94 ± 0.05	
D	3272vs (br)	NO	298 [28760]	285 [26 550]	305 [27 620]	4.17 ± 0.05	12.60 ± 0.19

NA = Not applicable; NO = Not observe; sh = sharp; br = broad; s = strong; vs = very strong.
[a] λ_{max} = the longest wavelength absorption peaks at the various protonation states.
[b] Solid state in KBr disc.
[c] In deuterated chloroform.
[d] ε could not be estimated due to lack of total conversion at these extremes of pH.
[e] S represents Standard error.

equilibrium species in a solution is known to render reliable results and the ionization constants can be obtained as pK_a values on the basis of Henderson-Hasselbalch theory [53]. The pK_a values were obtained from sigmoidal fittings on plots of absorbance values at selected wavelengths against pH (Fig. 1, inset) with R^2 values in the range 0.98–0.99. Some of the equilibria occurred at extremes of pH and only gave the onset of the sigmoidal plot as illustrated by Fig. 1(b) for ligand **A3** at the pH 14 end. Although the pK_a values for such equilibria could not be firmly estimated by spectroscopic methods, such plots show that the ionization constants are within the vicinity of the respective pH regions.

Comparing the longest wavelength absorption bands of the various ligands under similar protonation states, substitution of the methyl group at the *o*-position to the pyridyl N heteroatom did not yield any significant effects in the three series. This observation is supported by a similarity in the ^{1}H NMR and FTIR data of the 1H-imidazole active protons for the pairs **A1** and **A3**, **B1** and **B4**, and **C1** and **C3** (Table 1). However, substitution of the 1H-imidazole proton by a methyl group or the replacement of the imidazole ring by an oxazole ring increased the energies of the longest wavelength absorption bands in the **A** and **B** ligand series. Therefore, it could be concluded that the imidazole/oxazole ring possesses some influence on the electronic characteristics of the ligands in the **A** and **B** series. A similar comparison between imidazoles and oxazoles in the **C** series did not produce any notable changes, an indication that the electronic properties may depend less on the

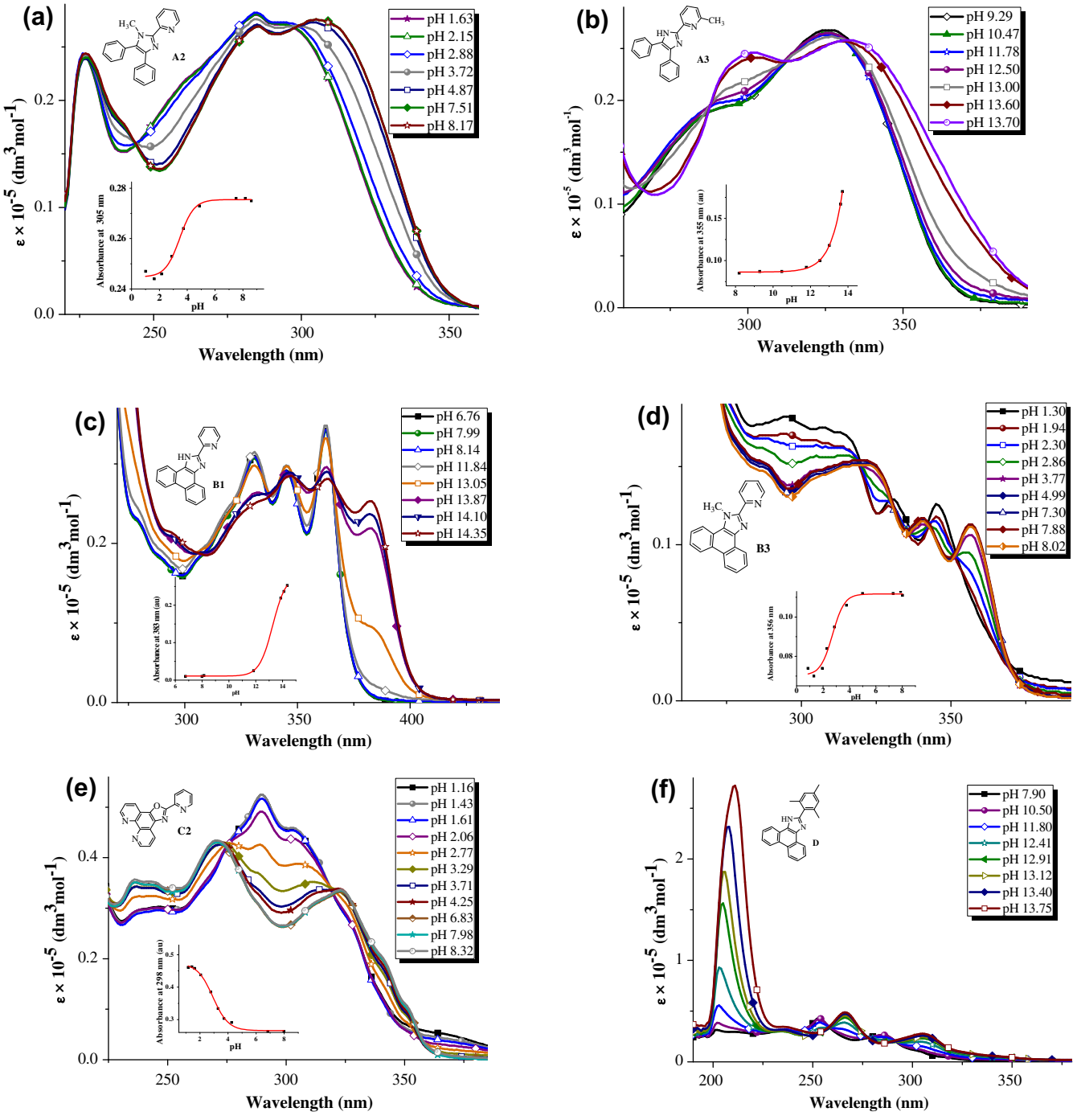

Fig. 1. Overlays of absorption spectra at different pH values; (a) **A2**, (b) **A3**, (c) **B1**, (d) **B3**, (e) **C2** and (f) **D**.

imidazole/oxazole heterocycle, but more on the phenanthroline heterocycles. All the ligands series **A** (305–326 nm), **B** (359–363 nm) and **C** (323–325 nm) gave longer absorption wavelengths than compound **D** (285 nm), which suggests the existence of greater conjugation from the imidazole/oxazole rings to the pyridyl ring as well as co-planarity of the imidazole/oxazole ring with pyridyl ring in the series **A**, **B** and **C** ligands. Absorption λ_{max} values indicate that the extent of such an extension of conjugation generally followed the order ligand **B** series > ligand **A** series > ligand **C** series > ligand **D**. It is noteworthy that slight changes in pH of the media between pH 12–14 resulted in ≈10-fold absorbance jump for the absorption band around 210 nm whilst having an insignificant effect on the longer wavelength bands (Fig. 1(f)).

3.2. Hemilability of imidazole-pyridyl/oxazole-pyridyl ligands from pK_a values

Scheme 2(a) and (b) shows a general sketch of the imidazole/oxazole skeleton at the various protonation states while Scheme 2(c) presents a descriptive numbering of atoms for which Mulliken charges were calculated and presented in Table 4. All imidazole ligands bearing the active N–H proton (Table 1: ligands **A1**, **A3**, **B1**, **B4**, **C1**, **C3**, **D**) exhibited two equilibria which consist of the protonation equilibrium of the N(3) base (Scheme 2(c)) in lower pH media (i.e. higher $[H^+]$, ≈pK_a 1–5) and the deprotonation reaction of the N(1) proton in higher pH environments (i.e. lower $[H^+]$, ≈pK_a 10–14). However, the oxazoles (Table 1: ligands **B2**, **B5**, **C2**, **C4**) as well as imidazoles in which the active proton has been substituted by a methyl group (Table 1: ligands **A2**, **A4**, **B3**) gave only one protonation–deprotonation equilibrium which corresponds to N(3) protonation in the lower pH 0–4 environments. This difference supports the assignment of pK_a 10–14 values in unsubstituted imidazole compounds to 1H-imidazole deprotonation events at higher alkalinities. The broad ^{1}H NMR and FTIR peaks that are commonly observed for 1H-imidazole protons are typical of ionizable protons (Table 1). Previous conclusions of 1H-imidazole deprotonation equilibria are also known for imidazo[4,5-f][1,10]phenanthrolines bound to Ru^{2+} (≈pK_a 8.0–9.0) [54,55]. Therefore, we concluded that the two types of equilibria observed in the ligand series involve the imidazole/oxazole rings rather than the pyridyl heterocycles and that the imidazole/oxazole moieties are substantially weaker Lewis bases relative to the pyridyl fragments. The requirement of larger $[H^+]$ (i.e. lower pH environments) for ligand protonation is an indication that the imidazole/oxazole rings possess poor donor strengths. Experimental data in this work suggest that protonation–deprotonation equilibria concerning the pyridyl bases (either at 2-imidazole carbon or on the phenanthrolinyl moieties), which are stronger Lewis bases, would occur substantially above pK_a 14 in 70% ethanol.

Participation of the oxo-atom on the oxazole ring in protonation–deprotonation equilibria was ruled out since it is considered to be a relatively poorer lone pair donor than the N(3) donor. The in-plane orientation for the N(3) donor lone pair is better positioned for donation, unlike the two lone pairs on the oxo-atom which would point at an angle to the aromatic oxazole plane. Reports on the acid dissociation constants of the Ru(II) complex of 2-(4-benzoxazolyl)phenylimidazo[4,5-f][1,10]phenanthroline ligand, which has a pendant benzoxazole unit, also concluded that the oxo-atom of the oxazole was not involved in any of the three reported protonation–deprotonation equilibria (≈pK_{a1} 1.70, pK_{a2} 5.23 and pK_{a3} 8.22) [56]. This view is further supported by scarcity of literature (if any exists) presenting M–O coordinated metal–oxazole compounds or intermolecular/intramolecular interactions between the oxo-atom of the oxazole ring and lone pair acceptors. In contrast, X-ray structures of free and even metal-coordinated 1H-imidazoles are commonly found with hydrogen-bonded networks involving the N(1) proton and the N(3) base [40,57,11].

3.3. Effect of substituents on imidazole/oxazole donor strengths

The strength of lone pair donation in the series of ligands could be compared on the basis of p$K_{a,N:}$ values (Table 1). Substituents with electron-withdrawing character on the basic nitrogen atom of the imidazole/oxazole ring would be expected to impart a reduction in the Lewis basicity, and vice versa. It was anticipated that conjugation between phenyl, phenanthrene or phenanthroline substituent groups and the imidazole/oxazole aromaticity would produce varying extents of charge density shift in the direction from the C(2) atom of the imidazole ring towards the C(4)–C(5) carbons on which the substituents are borne. Of all the investigated ligands, the **B** series ligands (phenanthrene substituted azoles) possessed the weakest imidazole/oxazole base donor characteristics. The general trend in donor abilities according to the p$K_{a,N:}$ of the ligand groupings is in the order **B** series (≈0–2.9) < **A** series (≈3.3–3.7) < **C** series (≈2.9–4.3). A notable observation is the fact that the observed trend suggests that the phenanthrenyl moiety is more electron withdrawing on the imidazole/oxazole ring than the phenanthrolinyl substituent, which is supported by sharper and stronger FTIR vibrational frequencies for **B1** (3433vs cm^{-1}) and **B4** (3436vs cm^{-1}) among the investigated ligand frameworks (Fig. 2(d); Table 1). This is the converse to the expected electronegativity influence of the N heteroatoms on the phenanthroline **C** series.

The substitution of 1H-imidazole positions by a methyl group, as in **A2**, **A4** and **B3**, was expected to produce an electron releasing influence towards the N(3) nitrogen base from the N(1) and consequently higher pK_as. However, it lead to slightly lower p$K_{a,N:}$ values compared to the unsubstituted imidazoles **A1**, **A3** and **B1**, respectively (Table 1). This suggests that methyl substitution facilitated a shift in electron density of the imidazole ring from the C(2) end to the C(4)–C(5) carbons on which the electron-withdrawing substituents are borne, leading to further reduction of charge density on the donor atom. Therefore, 1H-imidazole alkylation may not necessarily impart an increased donor strength on the N(3) hetero-

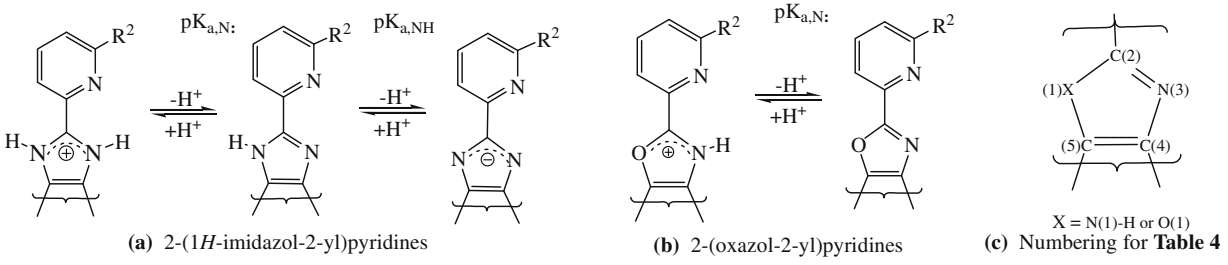

Scheme 2. Protonation–deprotonation equilibria for (a) imidazole rings, (b) oxazole rings within pH 0–14 environments and (c) descriptive atom numbering of the azole ring for reported charge densities in Table 4.

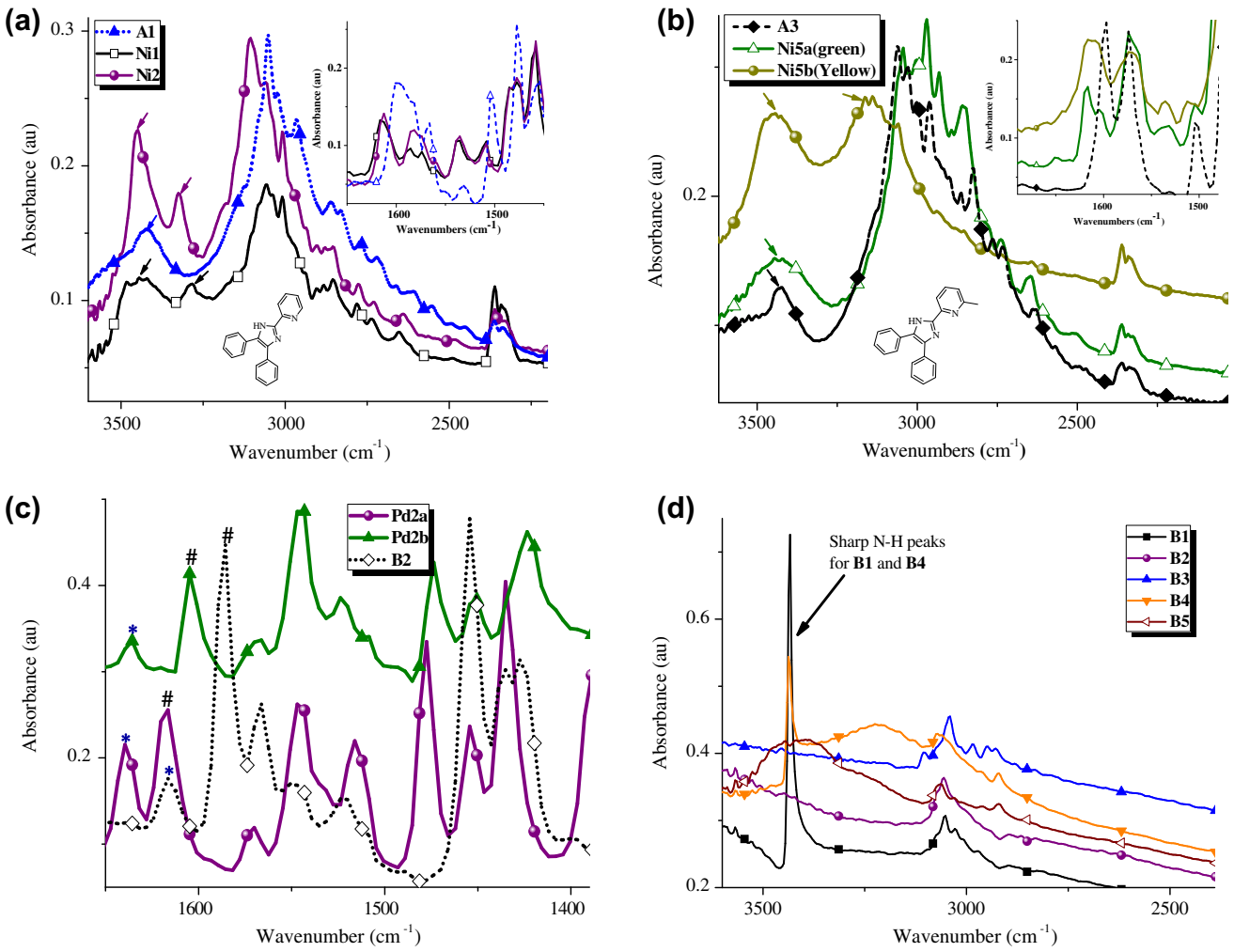

Fig. 2. Solid-state FTIR spectra (as KBr discs) of (a) nickel complexes with **A1**, (b) nickel complexes with **A3**, (c) palladium complexes with **B2** and (d) the **B** series ligands.

atom and electron density shifts across C(2) to the C(4)–C(5) axis is probably more important for tuning donor attributes of the imidazole base, as has been proposed for the 2-(1H-imidazol-2-yl)phenols which are prone to Excited State Intramolecular Proton-electron Transfer (ESIPT) [35].

However, replacement of the NH groups by an oxo-atom, as in the oxazoles **B2**, **B5**, **C2** and **C4**, yielded a notable reduction in the $pK_{a,N:}$ values of the respective imidazoles **B1**, **B4**, **C1** and **C3** understandably through the higher electronegativity of the oxo-atom (Table 1). According to the pK_a data, deprotonation of the **C** series imidazoles is easier than for the **B** series analogues, which supports the observed trends of phenanthrenyl substituent effects relative to the phenanthrolinyl analogue.

3.4. Supports from spectroscopic data of Ni(II) and Pd(II) complexes

One of the initial motivations for this work is the observation that oxazole **B5** formed a yellow complex with $NiCl_2{\cdot}6H_2O$, but the free ligand was readily precipitated in the presence of methanol. A summary of the preparation of the Ni(II) and Pd(II) complexes is presented in Scheme 3. The non-bridging 2-(imidazol/oxazol-2-yl)pyridine ligands (**A** and **B** series except ligand **B5**) reacted with dihalonickel(II) salts to give **Ni1**–**N9**, which have been previously characterized and applied to homogeneous olefin polymerization catalysis [41]. Ligands **A1** and **A2** only selectively formed the blue, bis-ligated nickel complexes, even when deliberate use of excess Ni(II) salt over 1:1 ratio was employed (Scheme 3;

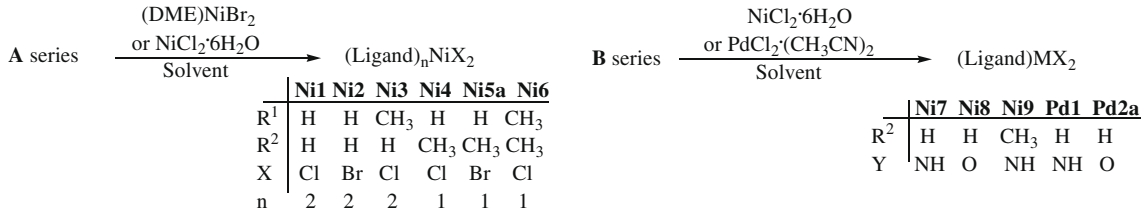

	Ni1	Ni2	Ni3	Ni4	Ni5a	Ni6
R^1	H	H	CH_3	H	H	CH_3
R^2	H	H	H	CH_3	CH_3	CH_3
X	Cl	Br	Cl	Cl	Br	Cl
n	2	2	2	1	1	1

	Ni7	Ni8	Ni9	Pd1	Pd2a
R^2	H	H	CH_3	H	H
Y	NH	O	NH	NH	O

Scheme 3. Summary of the reaction of Ni(II) and Pd(II) compounds with members of the **A** and **B** ligand series.

Table 2
Colour, FTIR ($\nu_{N=C,\ C=C}$) and melting/decomposition point data of the Ni(II) and Pd(II) compounds.

Compounds	Colour	$\nu_{N=C,\ C=C}$ (cm^{-1})	ν_{N-H}	Mp./Dp. (°C)
A1	White	1598, 1566	3422	174–176[d]
Ni1	Blue	1616, 1586	3443, 3285	>302[d,f]
Ni2	Blue	1612, 1581	3451, 3324	>312[d,f]
A2	White	1585, 1564		121–123[d]
Ni3	Blue	1605, 1573		>394[d,f]
A3	White	1597, 1574	3429	198–200[d]
Ni4	Yellow	1616, 1570	3380	>394[d,f]
Ni5a[a]	Green	1616, 1574	3431	242–244[e]
Ni5b[b]	Yellow	1612, 1572	3447, 3155	>300[e]
A4	White	1590, 1574		120–122[d]
Ni6	Yellow	1604, 1573		>214[d,f]
B1	White	1612m, 1592vs	3433vs(sh)	200–202[d]
Ni7	Yellow	1637w, 1609s	3394m(br)	>420[d,f]
Pd1	Orange	1631m, 1612vs	3490vs, 3395s	>300
B2	White	1617m, 1586vs		199–201[d]
Ni8	Green	1640vs, 1615s		>422[d,f]
Pd2a[a]	Orange	1639s, 1617vs		295–297[e]
Pd2b[c]	Brown	1636m, 1604s		>300[e]
B4	White	1616m, 1597s	3436s(sh)	218–220[d]
Ni9	Yellow	1604vs	3355s(br)	>390[d,f]
B5	White	1594m, 1569s		199–201[d]

s = strong; vs = very strong; m = medium; w = weak; sh = sharp.
[a] Crude product filtered from preparative reaction.
[b] Crystallized from MeOH layered with diethyl ether.
[c] Crystallized from DMSO.
[d] Data according to Ref. [41].
[e] Melting with decomposition.
[f] Decomposition.

Ni1–**Ni3**). However, ligands **A3** and **A4**, having $R^2 = CH_3$, and the phenanthrenyl ligands **B1**–**B4** formed the yellow 1:1 complexes (Scheme 3; **Ni4**–**Ni9**). These observations were established by X-ray structures for **Ni1**, **Ni3**, **Ni4** and **Ni9** in addition to elemental analysis of all the complexes [41]. Complexes of the **C** series ligands were not studied because all attempts to obtain a definite metal–organic architecture proved futile, with only polymeric products resulting. The appearance of two 1H-imidazole peaks around 3450 cm^{-1} and 3350 cm^{-1} for the bis-ligand complexes (**Ni1** and **Ni2**) suggests that the coordinated ligands exists in slightly different electronic environments, probably due to different hydrogen bonding environments in the solid state (Fig. 2(a); Table 2).

A notable observation is that coordination of the **A** and **B** ligand series to Ni(II) or Pd(II) metal centers lead to an increase in the vibrational frequencies assigned to the C=N/C=C double bonds for the coordinated ligands relative to the free ligands (Table 2; Fig. 2(a) and (b) inset for nickel; Fig. 2(c) for palladium). This phenomenon is contrary to the usual shift to lower wavenumbers in similar N-donor ligand frameworks, which is usually reported as a proof for ligand coordination to transition metals and is often attributed to increased electron delocalization that results from lone pair donation [58,59]. Consequently, the observation was considered to indicate a somewhat less favourable coordination for the imidazo-pyridine/oxazo-pyridine ligands compared with other well known bidentate ligands such as bipyridine and phenanthroline. It also suggests that this family of ligands may be useful for rational ligand exchange reactions and self-assembly protocols in

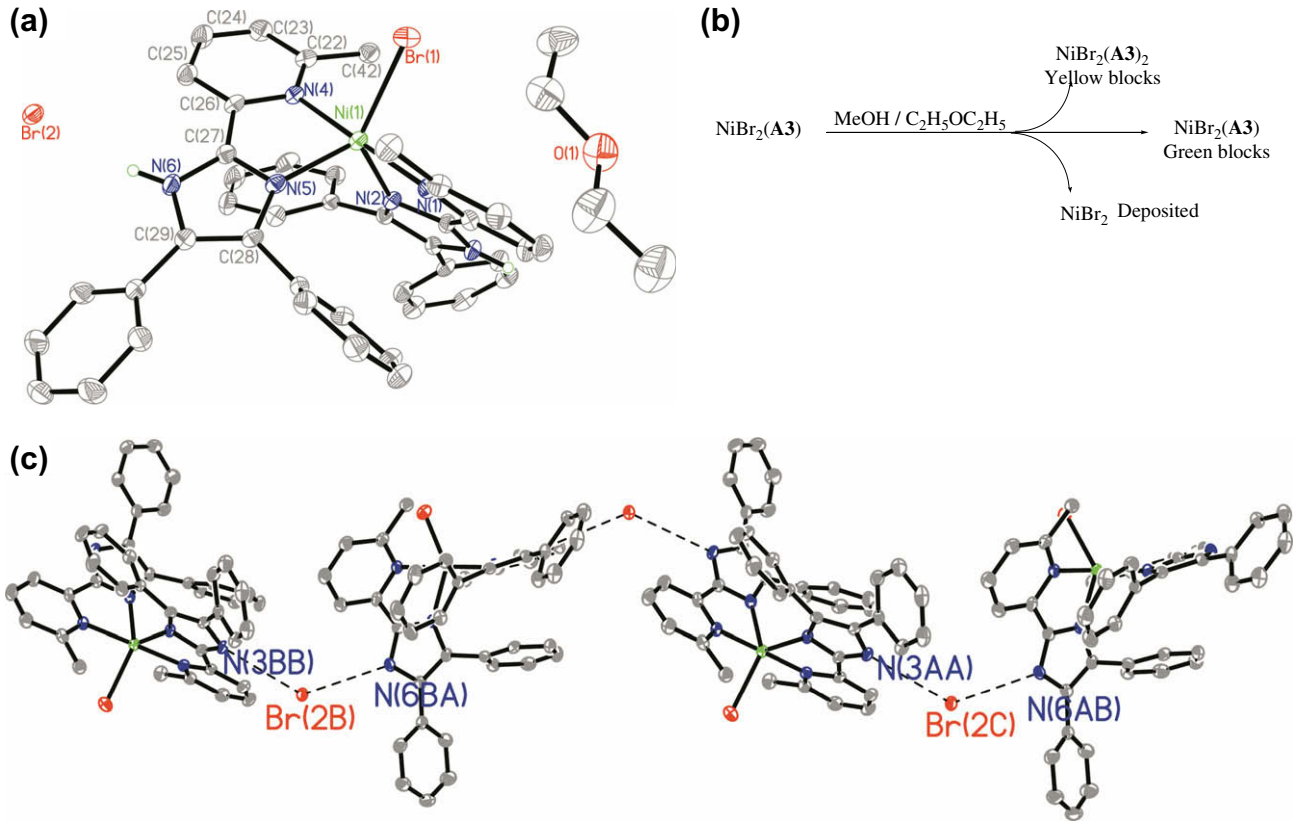

Fig. 3. (a) Ortep plot of complex **Ni5b** with thermal ellipsoids drawn at the 50% probability level, (b) proposed scheme for disproportionation and (c) the 1-dimensional hydrogen bonding network of the **Ni5b** cation and Br^-. Some atomic labels and protons have been omitted for clarity. Selected bond lengths (Å): Br(1)–Ni(1) = 2.4586(6); Ni(1)–N(5) = 2.023(2); Ni(1)–N(2) = 2.032(2); Ni(1)–N(1) = 2.097(2); Ni(1)–N(4) = 2.119(2). Selected bond angles (°): N(5)–Ni(1)–N(2) = 102.68(8); N(5)–Ni(1)–N(1) = 101.63(8); N(2)–Ni(1)–N(1) = 79.95(9); N(5)–Ni(1)–N(4) = 79.97(8); N(2)–Ni(1)–N(4) = 98.88(8); N(1)–Ni(1)–N(4) = 178.17(8); N(5)–Ni(1)–Br(1) = 130.66(6); N(2)–Ni(1)–Br(1) = 126.65(6); N(1)–Ni(1)–Br(1) = 88.33(6); N(4)–Ni(1)–Br(1) = 91.27(6). Hydrogen bonds parameters (Å and °): D–H···A = N(6BA)–H(6 N)···Br(2B); d(D–H) = 0.87(3); d(H···A) = 2.42(3); d(D···A) = 3.285(2); <(DHA) = 170(3); D–H···A = N(3BB)–H(3 N)···Br(2B); d(D–H) = 0.87(3); d(H···A) = 2.45(3); d(D···A) = 3.320(2); <(DHA) = 173(3).

the presence of common interacting solvents or other donors with comparable or higher ligand field strengths.

3.5. X-ray structures of the Ni(II) and Pd(II) complexes

Further evidence for the hemilability of the studied imidazo-pyridine/oxazo-pyridine ligands came from observed behaviours in solution of some of the complexes. It is noteworthy that all the yellow mono-ligated Ni(II) complexes dissolve in methanol to give dark green solutions from which green crystals typically precipitated in the presence of diethyl ether. The colour change from yellow to green in solution may be considered to be as a result of methanol coordination to vacant sites on the complexes, as observed in our published structure for **Ni4**. During attempts to obtain single crystals for **Ni5a** by dissolution of the complex in methanol and layering with diethyl ether via slow diffusion, a few sets of yellow crystal blocks of **Ni5b** were observed to grow as the diethyl ether solvate in the diethyl ether layer, in addition to the green blocks of **Ni5a** in the lower methanol layer, after a few days. **Ni5b** is believed to result from solvent mediated ligand disproportionation (Fig. 3(b)). Comparing the solid state FTIR data for **Ni5a** and **Ni5b** showed two peaks for active 1H-imidazole protons on **Ni5b** while only one peak was observed for **Ni5a** (Table 2, Fig. 2(b)). The observed difference is due to the mono-ligand structure of **Ni5a** compared to the bis-ligand structure for **Ni5b**, as shown in its Ortep plot (Fig. 3(a)). Selected bond lengths and angles around the metal center as well as hydrogen bonding parameters are presented along with the label of the figure. **Ni5b** shows a trigonal bipyramidal geometry around the nickel center. Br(1), N(2) and N(5) atoms form the trigonal plane, while N(1) and N(2) atoms occupied the axial positions (Fig. 3(a)). In comparison with other mono- and bis-ligand Ni(II) complexes of the **A** series ligands, the difference in melting/decomposition point data for **Ni5a** (242–244 °C) and **Ni5b** (>300 °C) is in line with their mono-ligand and bis-ligand structural identities, respectively (Table 2).

The compound **Pd2b** was also obtained during attempts to grow a suitable single crystal of **Pd2a**. **Pd2a** was dissolved in DMSO and layered with MeOH, in which the complex is insoluble. A single brown and large block of crystal was observed to have formed after about 2 weeks. However, it was observed that standing the saturated DMSO solution without layered solvent and without solvent evaporation also produced the same rectangular blocks of single crystals within a few days. Therefore, we conclude that **Pd2a** dissolves in and reacts with DMSO, leading to detachment of the oxazo-Pd bond and DMSO then coordinates to the palladium metal instead. The first significant difference between **Pd2a** and **Pd2b** is that **Pd2b** is insoluble in DMSO while the **Pd2a** is soluble. Hemilability of the ligand **B2** is believed to be confirmed from the structure of **Pd2b**, for which the Ortep plot is shown in Fig. 4. Comparative overlay of IR data for **Pd2a**, **Pd2b** and **B2** is presented in Fig. 2(c). The two $\nu_{N=C,\ C=C}$ bands for **B2**, 1617 and 1586 cm^{-1}, were shifted to higher wavenumbers by 23 and 29 cm^{-1}, respectively after coordination in **Pd2a**, and the detachment of the oxazo-palladium bond reversed the shift to lower wavenumbers after by 3 and 13 cm^{-1}, respectively. It appears that the 1586 cm^{-1} band pertains to vibrations on the 5-membered oxazole ring since it was more affected (13 cm^{-1}) after detachment of the oxazole-palladium coordination bond. Crystal data and processing parameters for **Ni5b** and **Pd2b** are presented in Table 3.

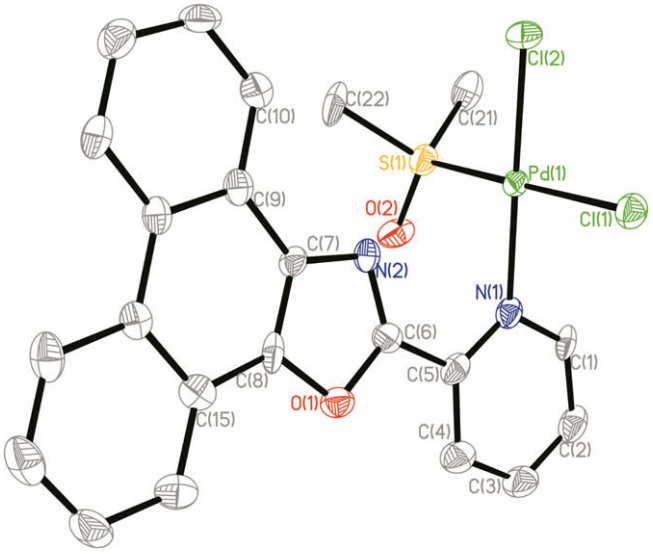

Fig. 4. Ortep plot of complex **Pd2b** with thermal ellipsoids drawn at the 50% probability level. Some atomic labels and protons have been omitted for clarity. Selected bond lengths (Å): Pd(1)–N(1) = 2.060(7); Pd(1)–S(1) = 2.246(2); Pd(1)–Cl(2) = 2.285(2); Pd(1)–Cl(1) = 2.318(2). Selected bond angles (°): N(1)–Pd(1)–S(1) = 91.24(19); N(1)–Pd(1)–Cl(2) = 179.2(2); S(1)–Pd(1)–Cl(2) = 89.59(8); N(1)–Pd(1)–Cl(1) = 88.05(18); S(1)–Pd(1)–Cl(1) = 175.20(8); Cl(2)–Pd(1)–Cl(1) = 91.12(8).

3.6. DFT calculation on the ligands

In an effort to further explore the experimental behaviours observed on account of ligand substituent effects, optimized geometries of all the organic ligands were calculated using GAUSSIAN 98 and properties such as the frontier orbitals as well as atomic charge densities were analyzed. The optimized structures revealed co-planarity between the imidazole/oxazole rings and the pyridyl rings attached to C(2), and loss of planarity for the **D** molecule (Fig. 5). The **B** series ligands generally possessed the lowest energy separa-

Table 3
Crystal data processing parameters for **Ni5b** and **Pd2b**.

	Ni5b·$C_2H_5OC_2H_5$	**Pd2b**·DMSO
Formula	$C_{46}H_{44}Br_2N_6NiO$	$C_{22}H_{18}Cl_2N_2O_2PdS$
Formula weight	915.40	551.74
T (K)	173(2)	173(2)
Wavelength (Å)	0.71073	0.71073
Crystal system	monoclinic	monoclinic
Space group	$P2(1)/n$	$C2/c$
a (Å)	16.842(3)	29.247(6)
b (Å)	14.284(3)	10.217(2)
c (Å)	17.359(4)	14.507(3)
α (°)	90	90
β (°)	95.71(3)	103.04(3)
γ (°)	90	90
V (Å^3)	4155.3(15)	4223.0(14)
Z	4	8
D_{Calc} (g cm^{-3})	1.463	1.736
μ (mm^{-1})	0.685	1.253
F(0 0 0)	1872	2208
Crystal size (mm)	0.27 × 0.23 × 0.15	0.37 × 0.27 × 0.19
θ Range (°)	3.27–27.48	1.43–27.47
Limiting indicates	$-21 \leqslant h \leqslant 21$ $-18 \leqslant k \leqslant 14$ $-22 \leqslant l \leqslant 14$	$-37 \leqslant h \leqslant 37$ $-13 \leqslant k \leqslant 13$ $-18 \leqslant l \leqslant 18$
Number of reflections collected	24 650	9116
Number of unique reflections	9479	4813
R(int)	0.0293	0.0276
Completeness to θ (%)	99.5% (θ = 27.48)	99.6% (θ = 27.47)
Number of parameters	517	273
Goodness-of-fit (GOF) on F^2	1.093	1.193
Final R indices ($I > 2\sigma(I)$)	R_1 = 0.0439 wR_2 = 0.0835	R_1 = 0.0852 wR_2 = 0.1947
R indices (all data)	R_1 = 0.0522 wR_2 = 0.0873	R_1 = 0.0997 wR_2 = 0.2032
Largest difference in peak and hole (e Å^{-3})	0.515, −0.490	0.550, −0.897

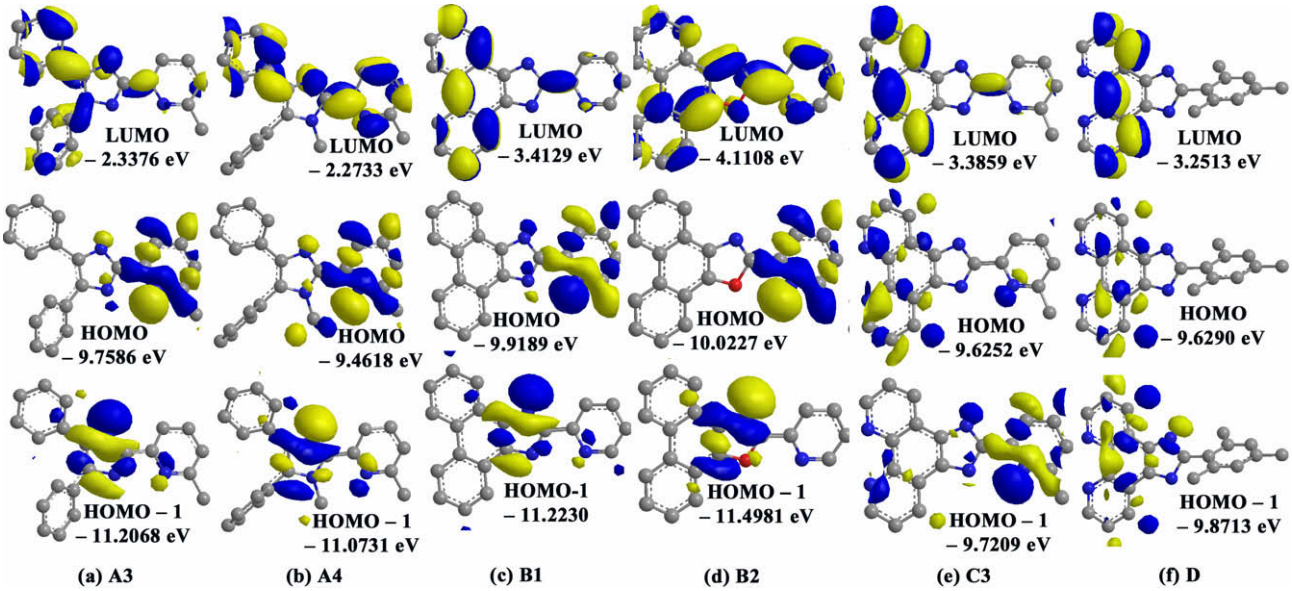

Fig. 5. Optimized structures of representative members of the various ligand groups showing the frontier molecular orbitals at the LUMO, HOMO and HOMO−1 levels. Hydrogen atoms are omitted for clarity.

Table 4
Ligand dipole moments, LUMO-HOMO separations and Mulliken charge densities of selected atoms determined at the B3LYP/6-311+G Level.

Ligands	$\Delta E_{(LUMO)-(HOMO)}$ (eV)[a]	Mulliken charge densities (Q)			
		N(3)	N(1)/O(1)	N(3)–N(1)	C(2)
A1	7.591	−0.401	−0.468	0.067	0.403
A2	7.285	−0.424	−0.764	0.340	0.423
A3	7.497	−0.401	−0.468	0.067	0.377
A4	7.173	−0.412	−0.763	0.342	0.407
B1	5.894	−0.381	−0.516	0.135	0.391
B2	5.912	−0.374	−0.476	0.102	0.330
B3	5.760	−0.404	−0.814	0.410	0.140
B4	5.758	−0.380	−0.516	0.136	0.117
B5	6.020	−0.373	−0.476	0.103	0.082
C1	6.233	−0.379	−0.512	0.133	0.090
C2	5.587	−0.373	−0.473	0.103	0.332
C3	6.239	−0.378	−0.513	0.135	0.371
C4	5.600	−0.372	−0.473	0.101	0.304
D	6.378	−0.365	−0.503	0.138	0.194

[a] LUMO = Lowest Unoccupied Molecular Orbital, HOMO = Highest Occupied Molecular Orbital (HOMO), eV = electron Volts. Selected atomic labels correspond to notations according to Fig. 4(b).

tions between the Highest Occupied Molecular Orbital (HOMO) and the Lowest Unoccupied Molecular Orbital (LUMO) ($\Delta E_{(LUMO)-(HOMO)}$, Table 4) which is in agreement with significantly lower energies of their longest wavelength bands (359–363 nm) compared with other ligands in this study (Table 1). Mulliken charge densities (Q) on atoms generally showed lower electron densities on the C(2) atoms as well as on N(3) donor atoms for the **B** series ligands compared to the other ligands. This tends to support the experimental suggestions on the stronger electron-withdrawing role of the phenanthrenyl substituent.

Finally, the frontier orbitals in all the molecules show the least activities for the imidazole/oxazole N(3) atoms compared to the considerably larger concentration of frontier orbitals on the pyridyl N donors (whether or not pyridyl of phenanthrolinyl; Fig. 5). Therefore, the computational data is in support of hemilability of 2-(1H-imidazol-2-yl)pyridines and 2-(oxazol-2-yl)pyridines. Considering the HOMO and HOMO−1 levels of the studied ligands, the calculations also support the importance of the imidazole/oxazole ring in the electronic energies of members of **A** and **B** ligand series (Fig. 5(a)–(d)). Dominance of the phenanthroline fragment on the electronic character of the HOMO levels in the **C** series is also supported by a concentration of the frontier orbitals on the phenanthroline end of the ligands (Fig. 5(e) and (f)).

4. Conclusion

Fourteen new organic molecules (**A1**–**A4**, **B1**–**B5**, **C1**–**C4** and **D**) and a series of transition metal(II) complexes (**Ni1**–**Ni9** and **Pd1**–**Pd2b**) were synthesized and studied in order to characterize the hemilability of 2-(1H-imidazol-2-yl)pyridines and 2-(oxazol-2-yl)pyridines and to explore trends caused by substituent effects on the donor strengths as well as coordination chemistries of imidazole/oxazole fragments of the hemilabile ligands. Protonation of imidazole/oxazole N donor atoms gave equilibria with pK_a values in the range 0–5, while deprotonation of imidazole active protons were characterized by pK_a values in the 10–14 range. The experimental results lead to the conclusion that all observed protonation–deprotonation processes observed within pH 1–14 media pertain to the 5-membered rings rather than the 6-membered pyridyl Lewis bases, and also that donor characteristics of the imidazole/oxazole ring can be estimated by spectroscopic methods regardless of the presence of other strong N donor fragments.

The low pK_a values demonstrate weak Lewis basicity of the 5-membered rings and hemilability of the chelate ligands as a whole. The donor strengths of the oxazoles are notably lower than those of imidazoles. The phenanthrenyl analogues (**B** series ligands) also possessed weaker donor strengths than their 4,5-diphenyl-substituted counterparts (**A** series ligands). It is noteworthy that, in disagreement with the expected greater electron-withdrawing influence of the phenanthroline heterocycle on the azole ring, basicity studies revealed stronger imidazole N donor qualities for the phenanthrolinyl ligands (**C** series) than for the phenanthrenyl analogues (**B** series), which indicates a greater electron-withdrawing influence for the phenanthrene substituent. It is also noteworthy that FTIR data for the complexes produced stronger $\nu_{N=C,\ C=C}$ vibrations for all the ligands after coordination to M(II) ions contrary to the usually reported shifts to lower wavenumbers after ligand coordination. The single crystal structures for **Ni5b** and **Pd2b** provided further evidence of ligand hemilability.

Interestingly, contrary to the popular expectation that alkylation of 1H-imidazoles would produce an increase in the ligand field strength of the imidazole ring, the experimental results showed that substitution of the 1H-imidazole position by an alkyl group did not necessarily produce the anticipated push of electron density across the imidazole ring to the donor nitrogen, but rather that electron density shifts from the C(2) carbon of the imidazole ring towards the C(4)–C(5) bond is probably more important for tuning the donor attributes of the imidazole base. Therefore, the substituent on the 4,5-carbon of the imidazole rings is more important in this regard. DFT calculations were carried out to probe the observed trends and provided some insight into the unusual behaviours. It is believed that the information provided on the substituent effects and trends in this family of ligands will be useful for the rational design and synthesis of desired azole-containing chelate ligands, tuning of donor properties and application of this family of ligands in inorganic architectural designs, template-directed coordination polymer preparations, mixed-ligand inorganic self-assemblies, etc.

5. Supplementary data

CCDC 758480 and 760817 contain the supplementary crystallographic data for **Ni5b** and **Pd2b**. These data can be obtained free of charge via http://www.ccdc.cam.ac.uk/conts/retrieving.html, or from the Cambridge Crystallographic Data Centre, 12 Union Road, Cambridge CB2 1EZ, UK; fax: (+44) 1223-336-033; or e-mail: deposit@ccdc.cam.ac.uk.

Acknowledgement

A.O.E. is grateful to Professor J.A. Emmanuel for useful ideas and to Redeemer's University – Nigeria for providing reagents and for granting study leave. The authors also thank the Chinese Academy of Sciences and the Academy of Sciences for the Developing World (Italy) for granting a postgraduate fellowship (CAS-TWAS) to A.O.E. Wen LI also thanks the National Natural Science Foundation of China for support of the research (Grant No. 20773149).

References

[1] A. Das, S.A. Trammell, M.H. Hecht, Biophys. Chem. 123 (2006) 102.
[2] F. Gao, X. Chen, F. Zhou, L.-P. Weng, L.-T. Guo, M. Chen, H. Chao, L.-N. Ji, Inorg. Chim. Acta (2009). doi:10.1016/j.ica.2009.07.034.
[3] I. Nobeli, S.L. Price, J.P.M. Lommerse, R. Taylor, J. Comput. Chem. 18 (1997) 2060.
[4] Y. Hu, X. Wang, R. Lu, Chem. Phys. Lett. 328 (2000) 337.
[5] R.S. Blake, P.S. Monks, A.M. Ellis, Chem. Rev. 109 (2009) 861.
[6] Y. Sato, Y. Onozaki, T. Sugimoto, H. Kurihara, K. Kamijo, C. Kadowaki, T. Tsujino, A. Watanabe, S. Otsuki, M. Mitsuya, M. Iida, K. Haze, T. Machida, Y. Nakatsuru, H. Komatani, H. Kotani, Y. Iwasawa, Bioorg. Med. Chem. Lett. 19 (2009) 4673.
[7] A.W. Kleij, Eur. J. Inorg. Chem. (Microreview), 2008. doi:10.1002/ejic.200800936.
[8] C. Foulon, C. Danel, C. Vaccher, S. Yous, J.-P. Bonte, J.-F. Goossens, J. Chromatogr. A 1035 (2004) 131.
[9] W. Lin, L. Long, L. Yuan, Z. Cao, B. Chen, W. Tan, Org. Lett. 10 (2008) 5577.
[10] W.N. Lipscomb, N. Strter, Chem. Rev. 96 (1996) 2375.
[11] Y.-P. Tong, S.-L. Zheng, X.-M. Chen, Eur. J. Inorg. Chem. 44 (2005) 3734.
[12] L. Bu, T. Sawada, Y. Kuwahara, H. Shosenji, K. Yoshida, Dyes Pigments 59 (2003) 43.
[13] G. Ataie, A.A. Moosavi-Movahedi, A.A. Saboury, G.H. Hakimelahi, J.R. Hwu, S.C. Tsay, Int. J. Biol. Macromol. 27 (2000) 29.
[14] L. Benisvy, A.J. Blake, D. Collison, E.S. Davies, C.D. Garner, E.J.L. McInnes, J. McMaster, G. Whittaker, C. Wilson, Chem. Commun. 2001 (2001) 1824.
[15] M.S.A. Hamza, X. Zou, R. Banka, K.L. Brown, R.v. Eldik, J. Chem. Soc., Dalton Trans. 2005 (2005) 782.
[16] B.F. Abrahams, B.F. Hoskins, R. Robson, J. Am. Chem. Soc. 113 (2005) 3603.
[17] M.J. Zaworotko, Chem. Commun. 2001 (2001) 1.
[18] O.M. Yaghi, H. Li, C. Davis, D. Richardson, T.L. Groy, Acc. Chem. Res. 31 (1998) 474.
[19] A.J. Blake, N.R. Champness, P. Hubberstey, W.-S. Li, M.A. Withersby, M. Schröder, Coord. Chem. Rev. 183 (1999) 117.
[20] S.R. Batten, R. Robson, Angew. Chem., Int. Ed. 37 (1998) 1460.
[21] S. Muthu, J.H.K. Yip, J.J. Vittal, J. Chem. Soc., Dalton Trans. 2002 (2002) 4561.
[22] T. Miyanaga, H. Sakane, I. Watanabe, J. Synchrotron, J. Rad. 8 (2001) 680.
[23] R. Fujiyoshi, T. Arai, M. Katayama, J. Radioanal. Nucl. Chem. 185 (1994) 133.
[24] D.K. Chand, R. Manivannan, H.S. Sahoo, K. Jeyakumar, Eur. J. Inog. Chem. 2005 (2005) 3346.
[25] J. Salvador, J.L. Garcé, E. Companys, J. Cecilia, J. Galceran, J. Puy, R.M. Town, J. Phys. Chem. A 111 (2007) 4304.
[26] D.A. Weinberger, T.B. Higgins, C.A. Mirkin, L.M. Liable-Sands, A.L. Rheingold, Angew. Chem., Int. Ed. 38 (1999) 2565.
[27] D.K. Chand, R. Manivannan, H.S. Sahoo, K. Jeyakumar, Eur. J. Inorg. Chem. 2005 (2005) 3346.
[28] H.M. Marques, J.C. Bradley, L.A. Campbell, J. Chem. Soc., Dalton Trans. 1992 (1992) 2019.
[29] V.C. Gibson, A.J. Graham, M. Jolly, J.P. Mitchell, J. Chem. Soc., Dalton Trans. 2003 (2003) 4457.
[30] J. Beckmann, D. Dakternieks, A. Duthie, C. Mitchell, J. Chem. Soc., Dalton Trans. 2003 (2003) 3258.
[31] T. Gladysheva, J. Liu, B.P. Rosen, J. Biol. Chem. 271 (1996) 33256.
[32] G.M. Protasiewyck, F.S. Nunes, Spectrochim. Acta A 65 (2006) 549.
[33] C. Foulon, N. Duhal, B. Lacroix-Callens, C. Vaccher, J.P. Bonte, J.F. Goossens, Eur. J. Pharm. Sci. 31 (2007) 165.
[34] M.G.B. Drew, C. Hill, M.J. Hudson, P.B. Iveson, C. Madic, L. Vaillant, T.G.A. Youngs, New J. Chem. 28 (2004) 462.
[35] A.O. Eseola, Nelson O. Obi-Egbedi, Spectrochim. Acta A 75 (2010) 693.
[36] K. Feng, F.-L. Hsu, D. van der Veer, K. Bota, X.R. Bu, J. Photochem. Photobiol. A: Chem. 165 (2004) 223.
[37] W.-H. Sun, P. Hao, S. Zhang, Q. Shi, W. Zuo, X. Tang, Organometallics 26 (2007) 2720.
[38] Q.-D. Liu, W.-L. Jia, S. Wang, Inorg. Chem. 44 (2005) 1332.
[39] D.B.G. Williams, T. Traut, F.H. Kriel, W.E. van Zyl, Inorg. Chem. Commun. 10 (2007) 538.
[40] A.O. Eseola, W. Li, R. Gao, M. Zhang, X. Hao, T. Liang, N.O. Obi-Egbedi, W.-H. Sun, Inorg. Chem. 48 (2009) 9133.
[41] A.O. Eseola, M. Zhang, J.-F. Xiang, W. Zuo, Y. Li, J.A.O. Woods, W.-H. Sun, Inorg. Chim. Acta, 2009. doi:10.1016/j.ica.2009.02.026.
[42] C. Öğretir, H. Berber, O. Asutay, J. Chem. Eng. Data 46 (2001) 1540.
[43] N.C. Marziano, C. Tortatoa, R. Bertani, Perkin Trans. 2 (1992) 955.
[44] G.T. Castro1, S.E. Blanco, O.S. Giordano, Molecules 5 (2000) 426–427.
[45] S. Kappaun, S. Horner, A.-M. Kelterer, K. Waich, F. Grasse, M. Graf, L. Romaner, F. Niedermair, K. Müllen, A.C. Grimsdale, R. Saf, E.J.W. List, E. Zojer, C. Slugovc, Macromol. Chem. Phys. 209 (2008) 2122.
[46] N. Dash, G. Krishnamoorthy, J. Fluoresc. 2009. doi:10.1007/s10895-009-0531-6.
[47] K. Das, N. Sarkar, A.K. Ghosh, J. Phys. Chem. 98 (1994) 9126.
[48] M.A. Rios, M.C. Rios, J. Phys. Chem. A 102 (1998) 1560.
[49] S. Yan, Y. Bu, Z. Cao, P. Li, J. Phys. Chem. A 108 (2004) 7038.
[50] M. Yamada, Y. Tanaka, Y. Yoshimoo, S. Kuroda, I. Shimao, Bull. Chem. Soc. Jpn. 65 (1992) 1006.
[51] M.J. Frisch, G.W. Trucks, H.B. Schlegel, G.E. Scuseria, M.A. Robb, J.R. Cheeseman, V.G. Zakrzewski, J.A. Montgomery Jr., R.E. Stratmann, J.C. Burant, S. Drapprich, J.M. Millam, A.D. Daniels, K.N. Kudin, M.C. Strain, O. Farkis, J. Tomasi, V. Barone, M. Cossi, R. Cammi, B. Mennucci, C. Pomelli, C. Adamo, S. Clifford, J. Ochterski, G.A. Petersson, P.Y. Ayala, Q. Cui, K. Morokuma, D.K. Malick, A.D. Rabuck, K. Raghavachari, J.B. Foresman, J. Cioslowski, J.V. Ortiz, B.B. Stefanov, G. Lui, A. Laishenko, P. Piskorz, I. Komoromi, R. Gomperts, R.L. Martin, D.J. Fox, T. Keith, M.A. Al-Laham, C.Y. Peng, A. Nanayakkara, C. Gonzalez, M. Challacombe, P.M.W. Gill, B. Johnson, W. Chen, M.W. Wong, J.L. Andres, C. Gonzalez, M. Head-Gordon, E.S. Repogle, J.A. Pople, GAUSSIAN 98, Revision A.6, Gaussian Inc., Pittsburgh, PA, 1998.
[52] G.M. Sheldrick, Acta Crystallogr. A A64 (2008) 112.
[53] A. Albert, E.P. Serjeant, The Determination of Ionization Constants, Chapman & Hall, USA, 1984. pp. 70–101.
[54] K.-Z. Wang, Inorg. Chem. Commun. 5 (2002) 841.
[55] Y. Pellegrin, R.J. Forster, T.E. Keyes, Inorg. Chim. Acta 2008. doi:10.1016/j.ica.2008.08.008.
[56] M.-J. Han, L.-H. Gao, Y.-Y. Lu, K.-Z. Wang, J. Phys. Chem. B 110 (2006) 2364.
[57] A. Quaranta, F. Lachaud, C. Herrero, R. Guillot, M.-F. Charlot, W. Leibl, A. Aukauloo, Chem. Eur. J. 13 (2007) 8201.
[58] M. Zhang, R. Gao, X. Hao, W.-H. Sun, J. Organomet. Chem. 693 (2008) 3867.
[59] R. Gao, M. Zhang, T. Liang, F. Wang, W.-H. Sun, Organometallics 27 (2008) 5641.